Viscoelastic Properties of the Ankle During Quiet Standing via Raster Images and EKF

Raul Chavez Romero, Antonio Cardenas, Davide Piovesan*, *Member, IEEE-EMBS*

***Abstract*—The present study deals with the reconstruction of the continuous-time state space parameters proper of human quiet standing. The reconstruction utilized a hybrid non-linear extended Kalman filter to combine a biomechanical model with the discrete-time position measurements provided by two web-cameras via a General Linear Camera model. After camera calibration and validating the filter in simulation, we performed the estimation on a group of volunteers whose quiet standing was perturbed by means of a hold and release paradigm. The filter allowed estimating stiffness and damping of the ankle during quiet standing as well as the kinematic variables of the subjects' center of mass.**

***Index Terms*—biomechanics, Extended Kalman Filter, joint stiffness, General Linear Camera model**

I. Introduction

The advent of video communication via internet protocols has favored the mass production of video-based system which nowadays can be acquired inexpensively. Furthermore, numerical algorithms that take into account the camera's optical model have allowed the adoption of raster image as a viable mean to estimate the position of objects in the three-dimensional Cartesian space [1]. When using a set of cameras to estimate the position of an object in space, the spatial resolution can be limited by the number of pixel of the photographic sensors. The knowledge of an accurate model of the camera is then necessary to reconstruct the position of an object in space based on its projection on the camera plane. This paper shows the possibility to achieve sub-pixel resolution by using an accurate camera model. In the proposed methodology, a linear regressive algorithm is used for the data fusion between the model and the measurement. We applied a general linear camera (GLC) model, previously utilized for the vision-based control of robotic devices [2], to a set of low-end web-cameras for estimating the postural stability of human quiet standing.

Understanding the mechanisms involved in postural stability is indispensable to improve the knowledge of how humans can regain balance against possible disturbances. Postural stability requires the ability to compensate the movement of the body's center of gravity caused by unexpected perturbations. The estimation of ankle mechanical impedance is an important tool used to gain insight on the interaction between biomechanics and the neural correlates proper of the control of postural stability [3]. Impedance is often modelled using a second order system, where the joint torques to resist a perturbation is a linear combination of acceleration, velocity, and angular displacements of the joints, and the coefficient of proportionalities are known as inertia, stiffness and damping [4].

In many engineering fields the use of Kalman filtering is widely spread to characterize the state matrix of linear systems for its characteristics of optimality and fast estimation. This paper proposes the identification of the stiffness and damping parameters of the ankle via the data fusion of a biomechanical model and the positional estimates obtained with a vision-based system. To this end we propose a time series analysis of the measurement by means of an extended Kalman filter (EKF) with augmented states. The perturbation to the biomechanical system is delivered using the hold and release paradigm as proposed by Bortolami and colleagues [5]. The advantages of EKF based methods are the possibility to have fast estimations on a single trial, offering the potential to estimate muscle and tendon stiffness during learning processes and adaptations on a trial by trial basis. The technique was tested on synthetic data to evaluate its precision and hence employed with living subjects.

II. Methods

A. Hold and Release Paradigm

The hold and release paradigm (H&R) is a technique to perturb the quiet standing of an individual, with the scope of exciting a neuro-mechanical response against falling [5]. Figure 1 illustrates the paradigm in detail.

In phase A the subject is in quiet standing and s/he is generating a torque at the ankle to counteract the torque generated by gravity as the center of mass is slightly forward with respect to the pivoting point at the ankle.

In phase B the experimenter applies a steady force, to the subject's sternum as to push her/him backwards. Hence, the subject produces a torque at the ankle to counteract the external load, which generates a torque around the same pivoting point. When the external load is suddenly removed in phase C the torque that was exerted by the subject to counteract the external load drives the body forward.

In phase D the fall is halted by the reaction of the neuro-mechanical systems through the application of a counteracting torque at the ankle. This is the instant after which the time series describing the position of the whole body center of gravity (COG) can be used in a system identification algorithm to identify the properties of human balance. Indeed, the subject is at its largest displacement far away from the equilibrium position. At this point we can hypothesize that the central nervous system (CNS) imposes a desired position command to bring the COG back to the equilibrium position as fast as possible. The command, as a first approximation, can be assume to be a step. The error between the desired angular position θ_f and the actual position induces the

[1] Raul Chavez Romero, Antonio Cardenas are with the Universidad Autónoma de San Luis Potosí (Mexico) and with Gannon University, Erie,PA, (USA). Davide Piovesan* is with Gannon University (e-mail: [romero005 , cardenas002; piovesan001]@gannon.edu). *Asterisk indicates corresponding author*. This work was partially supported by the Gannon University Faculty research Grant.

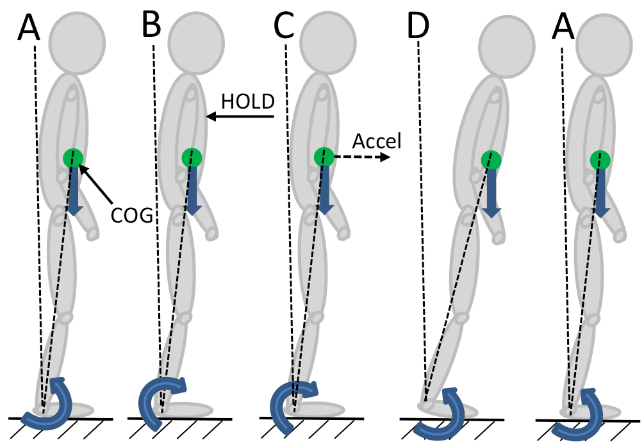

Fig. 1 A) Quiet standing. B) Hold. C) Release with consequence acceleration of the center of mass forward. D) Recoil where fall is prevented and quiet posture is regained as in condition A.

generation of a torque at the ankle via the neural-controller. The torque is applied to the muscle-skeletal system which moves toward the desired equilibrium position (Fig.1D-A). Thus, after a transient response, posture is finally stabilized as it was in phase A.

B. Hardware Description end experimental protocol

The apparatus to capture the H&R paradigm requires a system able to track the continuous change in position of the subject's center of mass. For this work we developed an affordable vision system to track the subject's center of mass position. We used a raster image acquisition system composed of two USB webcam Logitech c170 with definition of 640x480. The analysis and software interface was developed using Matlab 7.12.0. Two green fluorescent markers were placed onto each of the 16 neurologically intact subjects: one on the ankle to identify the center of rotation and one right above the navel. The placement of the latter marker is a good approximation of the subjects' center of gravity (COG) during quiet standing [6].

The subject positioned himself in a natural posture. The experimenter pushed the subject on the sternum while the subject tried to resist the perturbation. Hence a sudden release triggered the control reaction for recovering falls while the position of the COG was recorded by the vision based system.

C. Pinhole Camera Model and Estimation of 3D points

A linear relationship between points in three dimensional space and their projections in the plane of each camera sensor can be established based on the pinhole camera model. The mapping corresponding to the pinhole camera model is defined by a matrix C [3×4] formed by scalars, which has only 11 degrees of freedom (DOF) [1]. The C matrix can be decomposed in the following form:

$$C = K_c R_c [I \mid -D] \quad (1)$$

where I is the 3×3 identity matrix, D is the center of the camera with respect to a world reference frame, R_c is a rotation matrix in 3D, and K_c is the calibration matrix:

$$K_c = \begin{bmatrix} \alpha_x & S & p_x \\ 0 & \alpha_y & p_y \\ 0 & 0 & 1 \end{bmatrix} \quad (2)$$

where α_x and α_y correspond to the focal distance multiplied by an adjustment factor to consider the possibility that the sensor cells of the camera (CCD for example) are not squared, p_x and p_y are the coordinates of the principal point (center of the image) and S is the skew factor, which is zero if the axis of the sensor are orthogonal (normal case). The matrix K_c has 5 DOF and the matrices R and D have 3 DOF each summing up to a total of 11 DOF C.

The relationship between the point in $3D$ space and its projection in the image is well known in the robotics literature and it is given by the following equation [7]:

$$\begin{bmatrix} x \\ y \\ 1 \end{bmatrix} = \begin{bmatrix} c_1 & c_2 & c_3 & c_4 \\ c_5 & c_6 & c_7 & c_8 \\ c_9 & c_{10} & c_{11} & 1 \end{bmatrix} \begin{bmatrix} X \\ Y \\ Z \\ 1 \end{bmatrix} \quad (3)$$

where $[x, y]^T$ is the point in the image and $[X, Y, Z]^{\mathrm{T}}$ is the point in the world reference frame. Equation (3) can be rewritten as a linear system in the following manner [2]:

$$\begin{bmatrix} X & Y & Z & 1 & 0 & 0 & 0 & 0 & -xX & -xY & -xZ \\ 0 & 0 & 0 & 0 & X & Y & Z & 1 & -yX & -yY & -yZ \end{bmatrix} \mathrm{C} = \begin{bmatrix} x \\ y \end{bmatrix} \quad (4)$$

To calculate the matrix C at least 6 points are required ($i = 1,2,\ldots,6$). However, 5 points and the coordinate x or y of the sixth point are enough to find the analytical solution of the 11 parameters of vector C. If more than 6 points are used in computing C, an over constrained system is obtained and a minimization process is required to yield the solution. An over constrained system produces better results when estimating the vector C in the sense that the minimization process averages out the white noise in the estimation of the C parameters if the data number is large and the visual cues are located widely spread on the image plane.

Once the C parameters, have been obtained for at least two participating cameras, the target point $[X \quad Y \quad Z]^T$ can be estimated by solving the once redundant set of equations:

$$\begin{bmatrix} x^j \\ y^j \end{bmatrix} = \begin{bmatrix} c_1^j & c_2^j & c_2^j & c_4^j \\ c_5^j & c_6^j & c_7^j & c_8^j \end{bmatrix} \begin{bmatrix} X \\ Y \\ Z \\ 1 \end{bmatrix} \; for\ j = 1,2 \quad (5)$$

Where (x^j, y^j) represent the sampled camera-space location of the target point on camera j.

D. Static Calibration

To calibrate the vision system two cameras are positioned in two different fixed locations. Furthermore, a set of objects whose location is known in space is also required. The calibration was done positioning four checkerboard targets on each of the two orthogonal planes defined by a parallelepiped. The cameras where positioned so that both sides of the control volume could be in view (Fig. 2).

Each checkerboard has 6 X 8 squares where each square is 30 mm X 30 mm. The checkerboards were positioned pair-

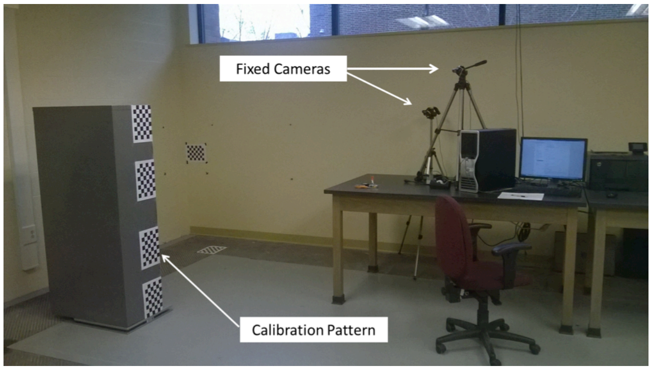

Fig. 2 Settings for calibrations pattern for estimation of vision parameters. Patterns were positioned pair-wise orthogonally to each other at four different hights. Only one pattern for each pair is visible.

wise orthogonally to each other at four different levels so to cover the positions in which shoulder, hip, knee and ankle are located for a person whose stature is 175cm (Fig. 2). A total of n=117 corners of each checkerboard pair were acquired by each camera, each representing a calibration point.

To assess the accuracy of the C parameters and the overall precision of this vision system, the C parameters were computed using only (n-1) points out of the n original points, the 3D position for the i^{th} point, which was left out from the n data points, was estimated. Then, an error was defined as the Euclidean distance between the actual 3D position of the point and its estimated position by the vision system so that an error was associated to that point. This process was repeated for all n points. The average error among all points was 1.89 mm with a standard deviation of 0.95 mm. The separation distance between the cameras and the calibration pattern was about 2.5 m and the pixel resolution was 4 mm/pixels which correspond to 0.0035 rad of angle resolution. Note that due to the least square regression described in section II.C it is possible to reach sub-pixel accuracy. With these results it was possible to conclude that a high profile camera for vision-machine applications was not required and off-the-shelf webcams with a 640 X 480 pixels resolution provide enough accuracy to estimate 3D points on a camera scene.

E. Measurement via Raster Images

Even though the movement of the subject in the H&R paradigm occurs approximately on a plane, when the static calibration is completed the cameras do not need to be relocated in order to be precisely aligned with a plane parallel to the movement. Two cameras can acquire any plane in 3D independently of the subject position. After the C parameters are calculated a linear mapping can be created between the position of any point in 3D space and their representations in the cameras' plane. The two green circular markers placed on the subjects' body were used as visual cues. The markers were identified within the camera space of both cameras by filtering all colors except green and then computing the centroid of the detected pixel clusters on camera space. Both visual markers positioned on the subject above the navel and on the ankle were detected by both cameras. Their corresponding 3D locations were estimated by using the position in camera space for each image as explained in section II.C. The time-series of the angular position between the secant line intersecting the two markers and a vertical line parallel to the direction of gravity was computed as the sum of the corresponding subtended arcs of an inverted pendulum tip between two consecutive instants.

F. Extended Kalman Filter Tuning and Parameter Estimation.

After obtaining the parameters of the GLC model, the position of the center of mass of each subject can be estimated in three-dimensional space. Hence the radius of gyration and the angle between the direction of gravity and the vector connecting the ankle with the COG can be estimated with simple trigonometry. Thus, as a first approximation, the biomechanical system describing quiet standing can be modeled as an inverted pendulum with one degree of freedom (DOF) (i.e. the rotation around the ankle) which can be represented by the following equation:

$$I_h\ddot{\theta} + b\dot{\theta} + k\theta = mgh \cdot \sin(\theta) + u + w_s \tag{6}$$

where for small oscillation $\sin(\theta) \cong \theta$, yielding:

$$I_h\ddot{\theta} + b\dot{\theta} + (k - mgh)\theta = u + w_s \tag{7}$$

where w_s is the uncertainties of the system modeled as a Gaussian noise, I_h is the inertia of the whole body with respect to the ankle, b is the damping coefficient, k is the stiffness, m is the mass of the subject, h is the radius of gyration of the subject and g is the acceleration of gravity. The term u is an additional external force. For this work $u = 0$ as the effect of gravity is already implemented as a constant stiffness mgh in equation (7). We can define an augmented state space model of equation (7) adding a number of states equal to the number of parameters that we want to estimate (i.e. b and k) so that the states are defined as $x_1 = \theta$, $x_2 = \dot{\theta}$, $x_3 = b + w_B$, $x_4 = k_s + w_K$ where $k_s = k - mhg$. The terms w_B and w_{K_s} are artificial noise terms that must be added to the system for each of the desired parameter (i.e. b and k_s) in order for the Kalman filter to modify their estimate [8]. Thus, the augmented state space system is defined by the following equation:

$$\dot{\mathbf{x}} = \begin{bmatrix}\dot{x}_1\\ \dot{x}_2\\ \dot{x}_3\\ \dot{x}_4\end{bmatrix} = \begin{bmatrix} x_2 \\ \frac{1}{I}(w_s - x_3x_2 - x_4x_1) \\ w_B \\ w_{K_s}\end{bmatrix} \tag{8}$$

and

$$\mathbf{w} = \begin{bmatrix} w_s \\ w_B \\ w_{K_s}\end{bmatrix} \tag{9}$$

we can apply a hybrid Extended Kalman filter, in the following form:

$$\begin{cases} \dot{\mathbf{x}} = \mathbf{f}(\mathbf{x}, \mathbf{w}, u, t) \\ \mathbf{y}_k = \mathbf{h}_k(\mathbf{x}_k, \mathbf{v}_k) \\ \mathbf{w} \sim (0, Q) \\ \mathbf{v}_k \sim (0, R_k) \end{cases} \tag{10}$$

where $\mathbf{w}$ and $\mathbf{v}$ are random noise of the augmented system $\mathbf{x}$ and the measurements vector $\mathbf{y}_k$ respectively, the subscript indicates the k discrete measurement acquired. The filter is initialized as follows:

$$\begin{cases} \hat{\mathbf{x}}_0^+ = E[\mathbf{x}_0] \\ P_0^+ = E[(\mathbf{x}_0 - \hat{\mathbf{x}}_0^+)(\mathbf{x}_0 - \hat{\mathbf{x}}_0^+)^T] \end{cases} \tag{11}$$

where circumflex is used to indicates the best estimates of a vector. The superscript "+" indicates that the current measurement has been considered for the estimation, whereas when the superscript is a "–" sign the last measurement has been not considered. From the initial values the following system can be defined

$$\begin{cases} \dot{\hat{\mathbf{x}}} = \mathbf{f}(\hat{\mathbf{x}}, \mathbf{0}, u, t) \\ \dot{P} = FP + PF^T + LQL^T \end{cases} \tag{12}$$

The numerical integration process begins with $\hat{\mathbf{x}} = \hat{\mathbf{x}}_{k-1}^+$ and $P = P_{k-1}^+$. At the end of this integration we have $\hat{\mathbf{x}} = \hat{\mathbf{x}}_k^-$ and $P = P_k^-$. So the next expressions can be calculated:

$$\begin{cases} K_k = P_k^- H_k^T (H_K P_k^+ H_k^T + R)^{-1} \\ \hat{\mathbf{x}}_k^+ = \hat{\mathbf{x}}_k^- + K_k\left(\mathbf{y}_k - \mathbf{h}_k(\hat{\mathbf{x}}_k^-, \mathbf{0}, t_k)\right) \\ P_k^+ = (I - K_k H_k) P_k^- (I - K_k H_k)^T + K_k R_k K_k^T \end{cases} \tag{13}$$

where $F = \left.\frac{\partial \mathbf{f}}{\partial \mathbf{x}}\right|_{\hat{\mathbf{x}},\mathbf{w}}$ and $L = \left.\frac{\partial \mathbf{f}}{\partial \mathbf{w}}\right|_{\hat{\mathbf{x}},\mathbf{w}}$, and $H_k = \left.\frac{\partial \mathbf{h}_k}{\partial \mathbf{x}_k}\right|_{\hat{\mathbf{x}}_k^-}$.

For the calibration of the EKF parameters synthetic data was built from the solution of (7). The synthetic data was created based on the experimental data. Thus, the position and velocity of the synthetic data was corrupted by Gaussian noise $\mathbf{w} \sim N(0,0.02)$, and a sampling rate of 10Hz was used in a time-series of 30 seconds. Finally some physiological parameters similar to the experimental data were used: $I_h = 100[Kg\, m^2/rad]$, $m = 80[Kg]$, $h = 1[m]$, $k = 1000[N\, m/rad\,]$, $g = 9.81[m/s^2]$, $k_s = k - mgh = 215.2$, $b = \sqrt{I_h k_s} = 146.6970$, $\mathbf{x}_0 = [0.1 \quad 0]^T$

Subsequently, the synthetic data is analyzed using the EKF in order to tune the filter parameters. The EKF was tuned using the following parameters:

$$P_0 = \begin{bmatrix} 1 & 0 & 0 & 0 \\ 0 & 1 & 0 & 0 \\ 0 & 0 & 100 & 0 \\ 0 & 0 & 0 & 100 \end{bmatrix}; \mathbf{x}_0 = \begin{bmatrix} 0 \\ 0 \\ 250 \\ 250 \end{bmatrix}; \tag{14}$$

$$Q = \begin{bmatrix} 0.1 & 0 & 0 \\ 0 & 0.1 & 0 \\ 0 & 0 & 0.1 \end{bmatrix}; R = \begin{bmatrix} 0.001 & 0 \\ 0 & 0.001 \end{bmatrix}.$$

Since 30 seconds of data sampled at 10 Hz is a limited amount of information to achieve convergence, we implemented a recursive algorithm where the filtering was repeated several times in the same set of data. For each iteration the last estimation of the parameters was used as an initial value for the next step until a difference between the initial conditions and the last estimation for both parameters b and k_s become less than 0.01.

III. Results

We can hypothesize that the movement of the COG is a direct consequence of the torque applied to the physical system to stabilize it. When the subject COG reaches the absolute maximum angular displacement with respect to the equilibrium position (-0.1rad circa) we are at the beginning of the recoil phase (Fig. 1D). From this point on, the condition is equivalent to a step in position as described in section II.A. The control system is reacting to drive the system back to its original equilibrium position. In Fig. 3 we can observe the angular displacement of the COG around the ankle with respect to the initial position for both the numerical simulation (left) and one representative subject (right). The estimation of velocity, damping *"b"* and stiffness *"k_s"* are also included. The error in the estimated value of the in-silico experiment are *Error_b* = 3.906 % and *Error_k_s*=1.47%.

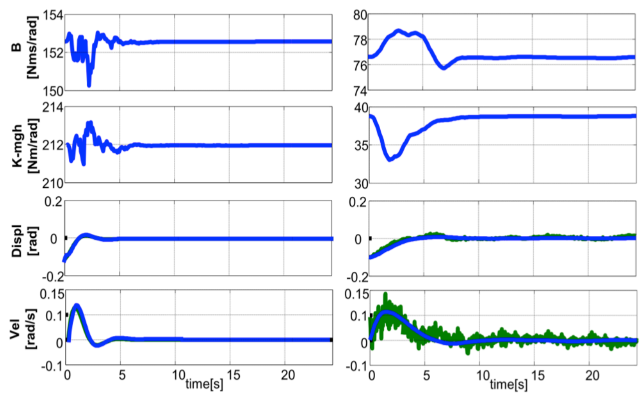

Fig. 3 transient in the recovery of fall between phase D and phase A in Figure 1. Green Line= experimental data. Blue line= EKF estimation. B=Damping; K=stiffness; m=subject mass; h= radius of gyration; g=gravity acceleration.Left Pannels: State estimation on synthetic data. Right Panels: Example of State estimation on experimetal data for a single representative individual.

By observing that all subjects were under-damped, we could measure the natural frequency of the system by means of a fast Fourier Transform (FFT). The ankle stiffness k can be easily calculated from the following relation:

$$(k - mgh) = I_h \omega_n^2 = mh^2 \omega_n^2 \tag{15}$$

where I_h is the moment of inertia with respect to the ankle, calculated as the mass m multiplied by the square of the distance h between the ankle and the position of the COG (i.e. the radius of gyration). This procedure gives us an approximate estimate of the ankle stiffness that can be compared with the EKF estimates. Table I shows that the average error between the two estimates is about 10.2%.

IV. Discussion and Conclusion

In this work we developed a motion capture system based on raster image. The two low-end commercial web-cameras were interfaced with a GLC algorithm that transforms the markers coordinates acquired in camera space to coordinates in Cartesian space. Furthermore, a biomechanical model of the human was integrated with the direct positional measurements from the cameras to reconstruct the tracked movements in the joint space and estimate the neuro-mechanical properties of the control of the ankle. When the system is approximated as second order, stiffness is the principal variable regulating the dynamic behavior of human movements and has been often considered as a figure of merit during the rehabilitation process from injuries and neuro-degenerative diseases [9-13]. The information from the joint angular displacements together with the estimation of stiffness and damping at the ankle could be utilized to estimate the dynamic behavior of the recovery to prevent falls.

In our experimental dataset we found that quiet standing was always subject to a residual vibration after perturbation. However, our research suggests that there exists a theoretical basis to expect a critically damped behavior [14]. One of the advantages of using an EKF instead of a frequency domain analysis is the possibility to identify the system even in over-damped conditions. Indeed, a frequency domain analysis requires a residual oscillation to be present, so that under the assumption of a second order model, the system has two complex conjugated poles [4, 15-17]. By using and EKF it is possible to estimate stiffness and damping even if the system has two real poles.

This approach can provide important experimental basis for the enhancement of dynamic simulations aimed at estimating muscle properties for human rehabilitation and performance improvement [18].

A limitation of the EKF presented here is the inherent assumption of a parametric model with time invariant parameters, where instead previously proposed time-frequency techniques tend to be very effective. Future work will focus on the estimation of parameter for a third order system where the stiffness of tendon and muscle can be estimated separately [19].

TABLE I
STIFFNESS AND INERTIAL PARAMETERS OF EACH SUBJECT

Num	Weight	Height	k_freq	k_EKF[Nm/rad]	Error
S1	88.45	1.80	1007.1	1076.9	6.9
S2	90.72	1.91	1253.7	1143.4	8.8
S3	76.66	1.73	852.3	778.5	8.7
S4	65.00	1.71	639.1	637.6	0.2
S5	65.00	1.65	792.9	842.2	6.2
S6	87.31	1.75	920.7	924.1	0.4
S7	106.14	1.75	1158.6	1151.0	0.7
S8	104.33	1.72	1101.0	1118.6	1.6
S9	69.85	1.70	998.4	1005.4	0.7
S10	116.21	1.85	1381.5	1348.3	2.4
S11	102.06	1.73	1827.6	1174.8	35.7
S12	68.04	1.71	811.4	764.8	5.7
S13	108.86	1.88	1073.1	1199.9	11.8
S14	80.65	1.80	972.3	1090.0	12.1
S15	100.61	1.75	1119.0	1263.1	12.9
S16	97.52	1.88	2032.2	1054.9	48.1

REFERENCES

[1] Z. Zhengyou, "A flexible new technique for camera calibration," *Pattern Analysis and Machine Intelligence, IEEE Transactions on,* vol. 22, pp. 1330-1334, 2000.

[2] A. Cárdenas, B. Goodwine, S. Skaar, and M. Seelinger, "Vision-Based Control of a Mobile Base and On-Board Arm," *The International Journal of Robotics Research,* vol. 22, pp. 677-698, September 1, 2003 2003.

[3] M. Casadio, P. G. Morasso, and V. Sanguineti, "Direct measurement of ankle stiffness during quiet standing: implications for control modelling and clinical application," *Gait & Posture,* vol. 21, pp. 410-424, 6// 2005.

[4] D. Piovesan, A. Pierobon, P. DiZio, and J. R. Lackner, "Measuring Multi-Joint Stiffness during Single Movements: Numerical Validation of a Novel Time-Frequency Approach," *PloS one,* vol. 7, p. e33086, 2012.

[5] S. B. Bortolami, P. DiZio, E. Rabin, and J. R. Lackner, "Analysis of human postural responses to recoverable falls," *Experimental Brain Research,* vol. 151, pp. 387-404, 2003/08/01 2003.

[6] P. M. McGinnis, *Biomechanics of Sport and Exercise*: Human Kinetics, 1999.

[7] R. Hartley and A. Zisserman, *Multiple View Geometry in Computer Vision*: Cambridge University Press, 2003.

[8] D. Simon, *Optimal State Estimation, Kalman, H_∞, and Nonlinear Approaches*. New Jersey: John Wiley & Sons, Inc, 2006.

[9] D. Piovesan, M. Casadio, F. Mussa-Ivaldi, and P. Morasso, "Multijoint arm stiffness during movements following stroke: Implications for robot therapy," in *Rehabilitation Robotics (ICORR), 2011 IEEE International Conference on*, 2011, pp. 1-7.

[10] D. Piovesan, M. Casadio, F. A. Mussa-Ivaldi, and P. Morasso, "Comparing two computational mechanisms for explaining functional recovery in robot-therapy of stroke survivors," in *Biomedical Robotics and Biomechatronics (BioRob), 2012 4th IEEE RAS & EMBS International Conference on*, 2012, pp. 1488-1493.

[11] A. Melendez-Calderon, D. Piovesan, and F. Mussa-Ivaldi, "Therapist recognition of impaired muscle groups in simulated multi-joint hypertonia," in *IEEE International Conference on Rehabilitation Robotics (ICORR)*, 2013, pp. 1-6.

[12] D. Piovesan, A. Melendez-Calderon, and F. Mussa-Ivaldi, "Haptic recognition of dystonia and spasticity in simulated multi-joint hypertonia," *IEEE International Conference on Rehabilitation Robotics,* vol. 2013, pp. 1-6, 2013.

[13] A. Melendez-Calderon, D. Piovesan, J. L. Patton, and F. A. Mussa-Ivaldi, "Enhanced assessment of limb neuro-mechanics via a haptic display," *Robotics and Biomimetics,* vol. 1, p. 12, 2014.

[14] D. Piovesan, C. J. Kennett, R. Chavez-Romero, M. C. Panza, and A. Cardenas, "Stiffness Boundary Conditions for Critical Damping in Balance Recovery," in *IEEE-ASME American Control Congress, ACC*, Chicago, 2014.

[15] D. Piovesan, P. Dizio, and J. Lackner, "A new time-frequency approach to estimate single joint upper limb impedance," in *Engineering in Medicine and Biology Society, 2009. EMBC 2009. Annual International Conference of the IEEE*, 2009, pp. 1282-1285.

[16] D. Piovesan, P. Morasso, P. Giannoni, and M. Casadio, "Arm stiffness during assisted movement after stroke: the influence of visual feedback and training," *Neural Systems and Rehabilitation Engineering, IEEE Transactions on,* vol. 21, pp. 454-465, 2013.

[17] D. Piovesan, A. Pierobon, P. DiZio, and J. R. Lackner, "Experimental measure of arm stiffness during single reaching movements with a time-frequency analysis," *Journal of neurophysiology,* vol. 110, pp. 2484-2496, 2013.

[18] R. Bortoletto, E. Pagello, and D. Piovesan, "Lower Limb Stiffness Estimation during Running: The Effect of Using Kinematic Constraints in Muscle Force Optimization Algorithms," in *Simulation, Modeling, and Programming for Autonomous Robots*, ed: Springer International Publishing, 2014, pp. 364-375.

[19] D. Piovesan, A. Pierobon, and F. A. Mussa Ivaldi, "Critical Damping Conditions for Third Order Muscle Models: Implications for Force Control," *Journal of Biomechanical Engineering,* vol. 135, pp. 101010-101010, 2013.